Proceedings of the 28th IEEE
EMBS Annual International Conference
New York City, USA, Aug 30-Sept 3, 2006

Subthalamic Nucleus Deep Brain Stimulation: Accurate Axonal Threshold Prediction with Diffusion Tensor Based Electric Field Models

[a,b]Ashutosh Chaturvedi, [a]Christopher R. Butson, [c]Scott E. Cooper, and [a,b,c]Cameron C. McIntyre
[a]Department of Biomedical Engineering, Cleveland Clinic Foundation, Cleveland, OH, USA
[b]Department of Biomedical Engineering, Case Western Reserve University, Cleveland, OH, USA
[c]Center for Neurological Restoration, Cleveland Clinic Foundation, Cleveland, OH, USA

***Abstract*-Deep brain stimulation (DBS) of the subthalamic nucleus (STN) has become the therapy of choice for medically intractable Parkinson's Disease. However, the physiological mechanisms responsible for the therapeutic effects of DBS remain unknown, and quantitative understanding of the interaction between the electric field generated by DBS and the underlying neural tissue is lacking. Recently our group has developed various computational techniques to study the neural response to DBS. The goal of this study was to incrementally incorporate increasing levels of complexity into our computer models of STN DBS and address activation of the corticospinal tract (CST). Our model system was customized to an STN DBS patient and CST thresholds were calculated with electric field models that ranged from an electrostatic, homogeneous, isotropic model to one that explicitly incorporated the capacitance of the electrode-tissue interface, tissue encapsulation of the electrode, and diffusion-tensor based 3D tissue anisotropy and inhomogeneity. The model predictions were compared to clinical CST thresholds defined from electromyographic recordings from eight muscle groups in the arm and leg of the STN DBS patient. Coupled evaluation of the model and clinical data showed that accurate prediction of axonal thresholds required our most detailed model. In addition, the simplifications and assumptions typically utilized in neurostimulation models substantially overestimate neural activation.**

I. Introduction

The subthalamic nucleus (STN) is an integral component of the basal ganglia and is known to play an important role in the pathophysiology of Parkinson's disease (PD) [1]. Chronic high frequency deep brain stimulation (DBS) of the STN has become an established therapy for the treatment of PD [2]. However, scientific understanding of the effects and mechanisms of DBS remains largely incomplete [3].

The fundamental purpose of DBS is to modulate neural activity with applied electric fields. However, most clinicians using DBS technology do not have a quantitative understanding of the effects of manipulating the various stimulation parameters on the neural response to the stimulation. Therefore, our group has worked to develop a wide range of computational models of DBS that address the volume of tissue activated by the stimulation [4, 5, 6, 7]. Our goal is to provide clinicians with an improved understanding of the effects of DBS, and to design stimulation experiments that address questions on the therapeutic mechanisms of DBS.

When building a model of a complex system, such as STN DBS, it is important to know the impact of various simplifications and assumptions on the predicative capabilities of the model. Typical neurostimulation electric field models assume electrostatic conditions and simplify the tissue medium to be homogeneous and isotropic. However, clinical DBS devices are placed within a highly anisotropic and inhomogenous tissue medium and they utilize voltage-controlled stimulation. Previously we have shown that under the conditions of voltage-controlled DBS, the capacitance of the electrode-tissue interface impacts the shape of the stimulus waveform transmitted to the tissue medium [6], and tissue encapsulation of the DBS electrode impacts the electrode impedance and the subsequent current delivered to the tissue medium [7]. In addition, the complex 3D tissue electrical properties of the STN region impact the shape of the electric field generated in the tissue medium [5]. The goal of this study was to address the impact of these various issues on stimulation predictions from an STN DBS model customized to an individual patient, and compare the model results to clinical activation thresholds.

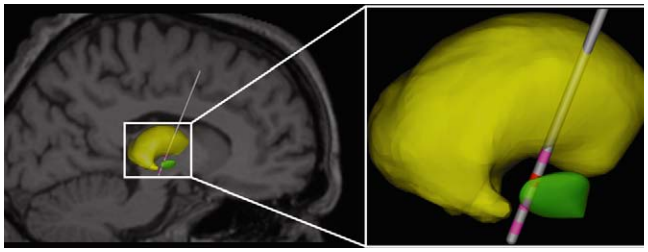

Fig. 1. Patient MRI scan with a 3D brain atlas warped to fit the thalamus (yellow) and STN (green). Right panel shows the position of the surgically implanted DBS electrode relative to the anatomical nuclei.

This study concentrated on STN DBS of the corticospinal tract (CST). The CST is a major fiber pathway within the internal capsule, which defines the lateral border of the STN. Consequently, motor evoked responses from activation of the CST can be elicited with relatively low thresholds during STN DBS. Clinically, CST activation is an unwanted side-effect of the stimulation. However, the generation of muscle contractions via stimulation of the CST represents a direct link between STN DBS, known neural substrates, and clinically measurable behaviors. Therefore, we used clinical measurements of CST activation to address the level of model complexity necessary to accurately predict neural activation generated by STN DBS.

II. Methods

This study used a highly detailed computer model of STN DBS in an individual patient. The model combined both

anatomical and diffusion tensor magnetic resonance imaging (MRI) data. The anatomical MRI was used to define the position of the DBS electrode in the patient's brain. The diffusion tensor MRI was used to define axonal trajectories of the CST. In addition, the diffusion tensor MRI was used to define 3D tissue anisotropy and inhomogeneity surrounding the DBS electrode. The electric field generated by STN DBS was calculated with a finite element model (FEM) that accounted for the capacitance of the electrode-tissue interface. In addition, the FEM incorporated an encapsulation sheath that surrounded the DBS electrode and regulated the electrode impedance. The electric field generated by the FEM was applied to multi-compartment cable models of myelinated axons. One hundred axon models were positioned within the anatomical context of the FEM such that they followed the path of the CST. Stimulation thresholds were calculated for action potential generation in the CST axon models using four variants of the FEM. Each FEM variant employed incremental levels of model complexity. The model results were then compared to clinically defined CST stimulation thresholds, with the goal of identifying the appropriate level of model complexity necessary to accurately represent STN DBS of the CST.

A. Clinical Data

The study received prior approval by the Cleveland Clinic Institutional Review Board, and the patient provided written informed consent. The male PD patient was implanted with bilateral STN DBS systems and exhibited good therapeutic benefit from the device. Pre- and post-operative high resolution T1 weighted MRIs were acquired. During the experimental testing, the patient was stimulated unilaterally with a 5 Hz, 120 μs pulse width cathodic waveform, with amplitudes of 1 V to 10 V in 1 V increments. Nine EMG electrodes were placed on the contralateral side of the body, and recordings were made from various muscles. One EMG electrode was placed on the neck over the subcutaneuous connector wire between the implanted pulse generator and the DBS electrode. This electrode detected the onset of the stimulus and was used as a trigger for signal averaging during the post-experiment analysis. The differential EMG recordings were averaged over 100 stimuli for each voltage increment, and the voltage thresholds for muscle contractions were determined using a stochastic signal-processing method [8].

B. Image Registration and Anatomical Nuclei

The pre- and post-operative MRI data were co-registered with a high resolution diffusion tensor brain atlas [9], using a mutual-information algorithm in Analyze 6.0 (Lenexa, KS). 3D representations of relevant anatomical nuclei (STN, thalamus, globus pallidus) were fit to the patient MRI data with a non-linear warping algorithm [10], using software developed by Surgical Navigation Technologies (Boulder, CO). The electrode tip location and trajectory were determined by segmenting out the electrode from the post-operative MRI using image thresholding. The anatomical and diffusion tensor MRI data, along with the anatomical nuclei and DBS electrode were all loaded into a common visualization and simulation platform developed by the Scientific Computing and Imaging Institute at the University of Utah (SCIrun/BioPSE).

C. CST Tractography

The CST fiber pathway was defined from the diffusion tensor brain atlas [9]. The individual interpolated tensors representing the internal capsule were used as a tracing guide from a seed point in the brain stem to a termination point near the dorsal thalamus. Using a total of five different seed point locations, five distinct fiber trajectories were created. These fiber trajectories were smoothed with a cubic spline function in Rhinoceros 3D (Seattle, WA). The five original fiber trajectories were then imported into a MATLAB (Natick, MA) script that generated 19 additional copies of each fiber. Each fiber copy had the same trajectory as the original fiber, except they were translated randomly in space. These translations were constrained such that no fiber would traverse through the STN, and that all copies of each unique fiber were displaced within ±2 mm in 3D from the original fiber trajectory. This methodology yielded 100 total fibers distributed within the internal capsule (Fig. 2).

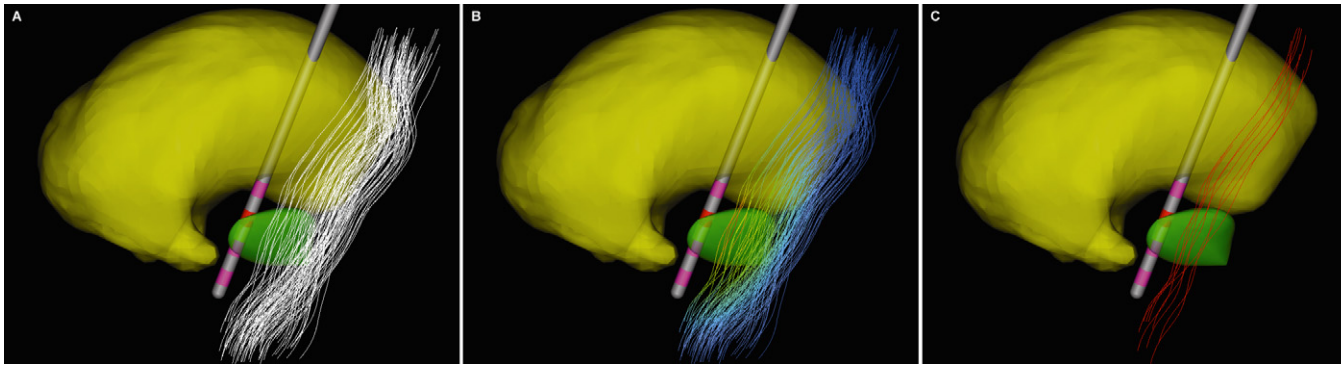

Fig. 2. Modeling and visualization environment. *A*: the thalamus (yellow), STN (green), DBS electrode, and the 100 randomly distributed CST fiber trajectories (white). *B*: The color map on the CST fibers describes the FEM voltage solutions impressed on those fibers with a 120 μs, -5 V cathodic stimulus waveform. Higher and lower stimulation voltages are shown in red and blue, respectively. The red contact on the DBS electrode shank depicts active contact 2. *C*: The nine CST fibers activated by the previous stimulus are shown in red.

D. Finite Element Electric Field Model

A multi-resolution finite element mesh of the DBS electrode and surrounding tissue medium was constructed using FEMLAB 3.1 (Comsol Inc., Burlington, MA). This mesh was imported into SCIrun/BioPSE and co-registered with the MRI data, anatomical nuclei, and CST fibers. In applicable simulations, the 3D tissue electrical properties of the brain were estimated from the diffusion tensor MRI data [5]. A simple linear transform was used to convert the diffusion tensor data into conductivity tensors [5, 11]. The Poisson equation was solved to determine the voltage distribution generated in the tissue medium by the DBS electrode. The simulations were performed on an 8-processor 32 GB shared memory SGI Prism (Mountain View, CA).

E. Coupling CST Fibers and the Electric Field

Multi-compartment cable models of myelinated axons, 5.7 μm in diameter, were created for each CST fiber [12]. The voltage solution from the FEM was interpolated onto each fiber trajectory. Simulations of the neural response to the applied field were preformed in NEURON 5.8 [13]. The stimulus waveform applied to the axon models was an asymmetrical charge-balanced pulse that mimicked the actual output of the Medtronic Itrel II (Minneapolis, MN) implanted pulse generator. In applicable simulations, the effects of the capacitance of the electrode-tissue interface were explicitly integrated into the shape of the stimulus waveform applied to the axon models [6]. Threshold was defined in each of the 100 fibers as the minimum stimulus voltage necessary to generate a propagating action potential.

E. Model Evaluations

CST activation during STN DBS was evaluated at the clinically defined therapeutic electrode contact (contact 2) on the right side of the brain. Four models, of increasing levels of complexity, were examined. The simplest model consisted of a homogeneous isotropic tissue medium with no electrode encapsulation, and stimulation was applied under electrostatic conditions. A slightly more complex second model integrated electrode capacitance (3.3 μF), which produced a more realistic waveform for stimulation [6]. The third model incorporated tissue encapsulation around the electrode, accounting for the chronic electrode impedance (1500 Ω) [7]. Finally, the most complex model added the diffusion tensor based 3D tissue conductivities.

III. Results

The stimulation voltage thresholds were determined for each CST fiber, along with their respective distances from the center of the stimulating contact on the DBS electrode (Fig. 3). Least-squares fits to the voltage-distance relationships from each model were generated with the following equation:

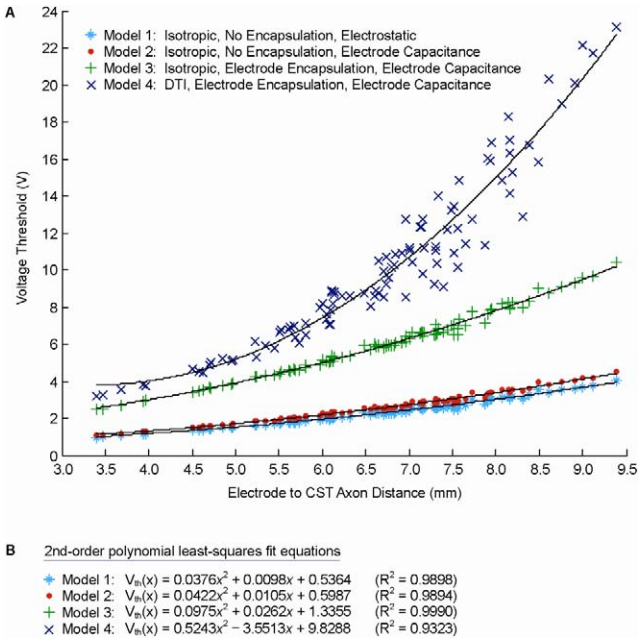

Fig. 3. Voltage thresholds versus electrode to CST axon distances for all four models. *A*: results from all models with 5 Hz, 120 μs, cathodic stimulation from therapeutic contact 2 on the patient's DBS electrode. *B*: least-squares fit equations for all four models, as well as their respective correlation coefficient R^2 values.

$$V\text{th} = Ax^2 + Bx + C, \quad (1)$$

where *V*th was the estimated threshold voltage necessary to activate a CST fiber, *x* was the electrode to fiber distance, and the constants A, B, C were calculated to give the best-fit to the data.

The clinical activation thresholds for various muscle groups were compared to the CST activations predicted by the models (Table 1). The more simplistic models predicted overwhelming activation of the CST. However, as the models became more complex, CST activation more realistically matched an expected level of 5-15% at a motor response threshold.

IV. Discussion

Clinically effective DBS electrodes are typically located in the posterior-lateral-dorsal STN [14, 15]. However, the

Muscle	Clinical activation	CST fibers activated (%)			
		Model 1	Model 2	Model 3	Model 4
Bicep	-4 V	99	96	13	5
Tricep	-7 V	100	100	78	25
FCU	-4 V	99	96	13	5
ECR	-6 V	100	100	53	16
Quadricep	-5 V	100	100	27	9
Ant. Tib.	-5 V	100	100	27	9
Lat. Gast.	-5 V	100	100	27	9

Table 1. Clinical threshold results and their respective model predictions for recruitment of CST fibers. FCU: flexor carpi ulnaris; ECR: extensor carpi radialis.

relatively small size of the STN (~10×10×8 mm) and the inherent inaccuracies of stereotactic neurosurgery, make exact placement of the permanently implanted DBS electrode in the target location difficult. In addition, the STN is surrounded by a number of fiber tracts, most notably the internal capsule (IC). The IC forms the lateral border of the STN, and stimulation spread into the IC is associated with a number of side effects of STN DBS. Therefore, clinical implementation of DBS technology is typically a balancing act between minimizing side effects and maximizing therapeutic benefit from the stimulation.

In this study we examined stimulation of the CST for two reasons. First, the generation of muscle contractions via stimulation of the CST represents a direct link between STN DBS, known neural substrates, and clinically measurable behaviors. In turn, we were able to make a close connection between our patient-specific model of STN DBS and clinical data recorded from that patient. Second, because CST activation is a common side effect of STN DBS it is important to understand the stimulation conditions that regulate its activation. Therefore, our results will help identify techniques to avoid CST activation in clinical DBS applications.

In an attempt to maximize the efficacy of DBS in individual patients, we have been developing techniques to predict the volume of tissue activated (VTA) by DBS. Our goal is to provide stimulation prediction information on a patient-specific basis and optimize the selection of stimulation parameters [8]. To achieve this goal we characterize the VTAs generated by therapeutic and non-therapeutic DBS, across a large number of patients, to develop a statistical database of stimulation spread. We then use that information to define therapeutic target volumes of tissue that we use to predict theoretically optimal stimulation parameter settings for DBS in new patients [16]. This system requires a stimulation prediction model that accurately captures the neural response to DBS. The purpose of this study was to evaluate the level of model complexity necessary to achieve our goals.

Our simulation results suggest that the VTA generated by DBS depends on a long list of factors including: 1) electrode capacitance, 2) electrode impedance, 3) electrode location and orientation in the brain, and 4) 3D tissue conductivity surrounding the electrode. We have developed the computational infrastructure necessary to account for all of these factors. The results of this study suggest that accurate estimation of the neural response to DBS requires a model that incorporates all of these factors.

ACKNOWLEDGEMENT

This work was supported by grants from the American Parkinson Disease Association, the Ohio Biomedical Research and Technology Transfer Partnership, and the National Institutes of Health (NS-50449 & NS-52042). The authors would also like to thank Jaimie Henderson for providing the 3D anatomical models, Susumu Mori for providing the diffusion tensor image brain atlas, Christopher Maks and Svjetlana Miocinovic for assistance with the model simulations, and Barbara Wolgamuth for assistance the clinical threshold data collection.

REFERENCES

[1] Bergman H, Wichman T, Karmon B, and DeLong MR. The primate subthalamic nucleus. II. Neuronal activity in the MPTP model of parkinsonism. *Journal of Neurophysiology* 1994; 72: 507-20.

[2] Obeso JA, Olanow CW, Rodriguez-Oroz MC, Krack P, Kumar R, and Lang AE. Deep-brain stimulation of the subthalamic nucleus or the pars interna of the globus pallidus in Parkinson's disease. *New England Journal of Medicine* 2001; 345: 956-63.

[3] McIntyre CC, Savasta M, Kerkerian-Le Goff L, and Vitek JL. Uncovering the mechanism(s) of action of deep breain stimulation: activation, inhibition, or both. *Clinical Neurophysiology* 2004; 115: 1239-48.

[4] McIntyre CC, Grill WM, Sherman DL, and Thakor NV. Cellular effects of deep brain stimulation: model-based analysis of activation and inhibition. *Journal of Neurophysiology* 2004; 91(4): 1457-69.

[5] McIntyre CC, Mori S, Sherman DL, Thakor NV, and Vitek JL. Electric field and stimulating influence generated by deep brain stimulation of the subthalamic nucleus. *Clinical Neurophysiology* 2004; 115: 589-95.

[6] Butson CR, and McIntyre CC. Tissue and electrode capacitance reduce neural activation volumes during deep brain stimulation. *Clinical Neurophysiology* 2005; 116: 2490-2500.

[7] Butson CR, Maks CB, and McIntyre CC. Sources and effects of electrode impedance during deep brain stimulation. *Clinical Neurophysiology* 2006; 117(2): 447-54.

[8] Butson CR, Cooper SE, Henderson JM, and McIntyre CC. Patient-specific analysis of the volume of tissue activated during deep brain stimulation. *NeuroImage*, (submitted for review).

[9] Wakana S, Jiang H, Nagae-Poetscher LM, van Zijl PCM, and Mori S. Fiber tract-based atlas of human white matter anatomy. *Radiology* 2004; 230: 77-87.

[10] Christensen GE, Joshi SC, and Miller MI. Volumetric transformation of brain anatomy. *IEEE Transactions on Medical Imaging* 1997; 16(6): 864–77.

[11] Tuch DS, Wedeen VJ, Dale AM, George JS, and Belliveau JW. Conductivity tensor mapping of the human brain using diffusion tensor MRI. *Proceedings of the National Academy of Sciences of USA* 2001; 98(20): 11697-701.

[12] McIntyre CC, Richardson AG, and Grill WM. Modeling the excitability of mammalian nerve fibers: influence of afterpotentials on the recovery cycle. *Journal of Neurophysiology* 2002; 87(2): 995-1006.

[13] Hines ML, and Carnevale NT. The NEURON simulation environment. *Neural Computing* 1997; 9:1179-1209.

[14] Saint-Cyr JA, Hoque T, Pereira LC, Dostrovsky JO, Hutchison WD, Mikulis DJ, Abosch A, Sime E, Lang AE, and Lozano AM. Localization of clinically effective stimulating electrodes in the human subthalamic nucleus on magnetic resonance imaging. *Journal of Neurosurgery* 2002; 97(5): 1152-66.

[15] Nowinski WL, Belov D, Pollak P, and Benabid AL. A probabilistic functional atlas of the human subthalamic nucleus. *Neuroinformatics* 2005; 2(4): 381-98.

[16] Butson CR, Maks CB, Cooper SE, Henderson JM, and McIntyre CC. Deep brain stimulation interactive visualization system. *Society for Neuroscience* 2005; 898.7.